

Water Molecules in the Binding Cavity of Intestinal Fatty Acid Binding Protein: Dynamic Characterization by Water ^{17}O and ^2H Magnetic Relaxation Dispersion

Silke Wiesner¹, Elizabeth Kurian², Franklyn G. Prendergast² and Bertil Halle^{1*}

¹Condensed Matter Magnetic Resonance Group, Department of Chemistry, Lund University PO Box 124, S-22100 Lund Sweden

²Department of Biochemistry and Molecular Biology, Mayo Foundation, Rochester, MN 55905, USA

The hydration of intestinal fatty acid binding protein (IFABP) in apo-form and complexed with palmitate, oleate, and 1-anilino-8-naphthalene sulfonate (ANS) has been studied by water ^{17}O and ^2H magnetic relaxation dispersion (MRD) measurements. These ligands bind in a large internal cavity, displacing most of the crystallographically identified cavity water molecules. Unlike most other proteins, IFABP gives rise to MRD profiles with two dispersion steps. The low-frequency dispersion yields a correlation time of 7 ns at 300 K, matching the known tumbling time of IFABP. The dispersion amplitude requires only three (apo) or four (holo) long-lived and ordered water molecules (residence time 0.01–4 μs at 300 K). Comparison of MRD profiles from the different complexes indicates that the displaced cavity water molecules are short-lived. The few long-lived (>10 ns) water molecules required by the MRD data are tentatively assigned to crystallographic hydration sites on the basis of accessibility, positional order, and H-bonding. The amplitude of the high-frequency dispersion corresponds to 10–20 moderately ordered water molecules, with a correlation time of ca. 1 ns that may reflect a transient opening of the cavity required for exchange with external water.

© 1999 Academic Press

*Corresponding author

Keywords: intestinal fatty acid binding protein; magnetic relaxation dispersion; protein hydration; water residence time; cavity

Introduction

Intestinal fatty acid binding protein (IFABP) belongs to the family of intracellular lipid binding proteins (iLBPs), responsible for intracellular uptake and translocation of long-chain fatty acids and other sparingly soluble polar lipids. The iLBPs may also be involved in lipid metabolism, signal transduction, and modulation of cell growth and differentiation (Glatz & van der Vusse, 1996). Like most other iLBPs, IFABP binds a single fatty acid molecule with high affinity in a large internalized cavity lined by two five-

stranded antiparallel β -sheets and capped on one side by two short α -helices (Figure 1; Sacchettini & Gordon, 1993; Banaszak *et al.*, 1994). High-resolution crystal structures (Sacchettini *et al.*, 1989a, 1992; Scapin *et al.*, 1992; Eads *et al.*, 1993), as well as NMR solution structures (Hodsdon *et al.*, 1996; Hodsdon & Cistola, 1997a; Kurian, 1998) are available for both apo and holo forms of rat IFABP and the binding thermodynamics (Richieri *et al.*, 1995, 1997, 1998; Kirk *et al.*, 1996; Kurian *et al.*, 1996) and kinetics (Richieri *et al.*, 1996; Cistola *et al.*, 1996) have been characterized for wild-type IFABP and several mutants. Yet, neither the molecular basis of binding affinity and specificity, nor the mechanism of fatty acid binding and release is well understood.

In the 1.2 Å crystal structure of apo-IFABP, 22 water molecules are found in the binding cavity (Scapin *et al.*, 1992). In the presence of bound fatty acid, only eight water molecules are detected in the cavity (Figure 1), but the holo-protein is otherwise nearly indistinguishable from

Abbreviations used: ANS, 1-anilino-8-naphthalene sulfonate; HFABP, heart muscle fatty acid binding protein; IFABP, intestinal fatty acid binding protein; iLBP, intracellular lipid binding protein; MD, molecular dynamics; MRD, magnetic relaxation dispersion; NOE, nuclear Overhauser effect; NOESY, nuclear Overhauser effect spectroscopy.

E-mail address of the corresponding author: bertil.halle@fkem2.lth.se

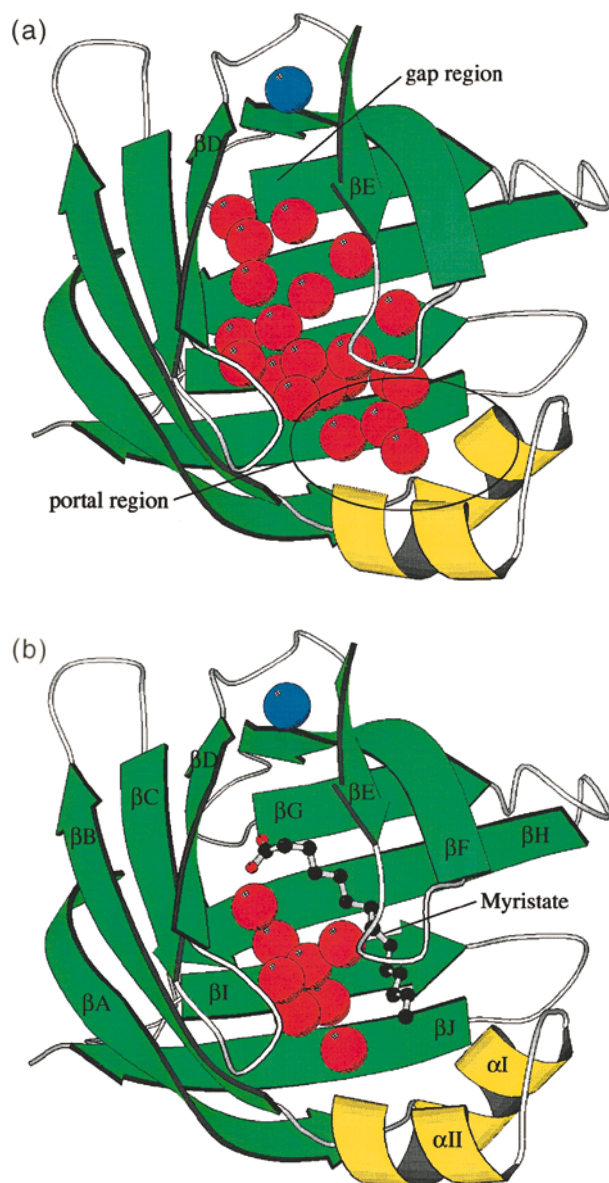


Figure 1. Crystal structures of (a) apo-IFABP (PDB code 1ifc) and (b) holo-IFABP with bound myristate (1icm) showing the two orthogonal β -sheets (green), the two short α -helices (yellow), the fatty acid (holo), 22 (apo) or eight (holo) water molecules (red) buried within the cavity, and one water molecule (blue) buried elsewhere (W135 in apo, W134 in holo). The locations of the gap region, between β -strands D and E, and the proposed portal for fatty acid entry into the cavity are also indicated.

suggested that the release of ordered cavity water molecules enhances the binding affinity (Sacchettini *et al.* 1989b; Sacchettini & Gordon, 1993), but the associated entropy changes have not been quantified. A small opening, the "portal", and a side-chain-filled β -sheet defect, the "gap", have both been implicated (Sacchettini & Gordon, 1993; Banaszak *et al.*, 1994) as possible pathways for exchange of fatty acid and water between the cavity and the external medium (Figure 1). These exchange processes are presumably coupled to protein conformational dynamics (Hodsdon & Cistola, 1997a,b), but little is known about the rates and amplitudes of such conformational fluctuations. In particular, no experimental data are available on the mobility and exchange rates of the water molecules in the IFABP cavity.

Detailed information about cavity hydration in proteins in solution can be obtained with two complementary NMR techniques, utilizing the magnetic relaxation dispersion (MRD) of the water isotopes ^{17}O and ^2H (Halle *et al.*, 1999) and the intermolecular nuclear Overhauser effect (NOE) between protein and water protons (Otting, 1997). A water-NOE study of FABP from heart muscle (HFABP) was recently reported (Mesgarzadeh *et al.*, 1998) and a similar study of IFABP has been completed (V. A. Likic, N. Juranic, S. Macura & F. G. Prendergast, unpublished results). Here, we report the first application of the MRD technique to a protein in the iLBP family. MRD data provide information about orientational order and residence times of long-lived hydration water molecules, but do not provide their locations. With the aid of high-resolution crystal structures and difference-MRD experiments, however, the dynamic information can often be related to specific hydration sites (Halle *et al.*, 1999). We have thus compared MRD data from apo-IFABP and holo-IFABP with bound palmitate, oleate, and 1-anilino-8-naphthalene sulfonate (ANS).

The results shed new light on the role of cavity water molecules for fatty acid binding to IFABP and on the kinetics of water exchange from the cavity. In particular, we conclude that only one or two cavity water molecules are long-lived, with a residence time in the range 0.01–4 μs at 27 $^{\circ}\text{C}$. Most of the cavity water molecules have a residence time of about 1 ns, which we tentatively identify as the time scale for protein conformational fluctuations that partially expose the internal binding cavity. The MRD results also indicate that holo-IFABP contains more cavity waters than detected by X-ray crystallography.

Results

Overview of MRD results

We have measured the water ^{17}O and ^2H longitudinal relaxation dispersion profiles in the 1–100 MHz range for IFABP in the apo form and in com-

the apo-protein (Sacchettini & Gordon, 1993). While hydrated internal cavities are a generic feature of globular proteins (Rashin *et al.*, 1986; Williams *et al.*, 1994; Baker, 1995), the IFABP cavity is particularly intriguing because of its exceptional size and obvious functional role. It is not clear why the fatty acid binds to an aqueous cavity three times its own size rather than to a tight-fitting hydrophobic surface crevice. It has been

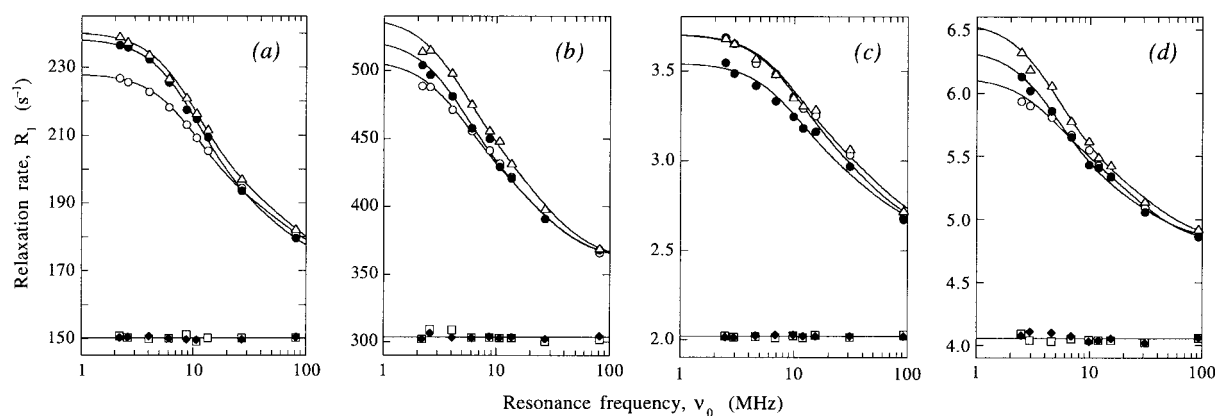


Figure 2. Frequency dependence of the water ¹⁷O ((a) and (b)) and ²H ((c) and (d)) longitudinal relaxation rate in solutions of apo-IFABP (○), oleate-IFABP complex (●), and ANS-IFABP complex (△) at 27 °C ((a) and (c)) and 4 °C ((b) and (d)). All data refer to 2.12 mM IFABP from batch I at pH* 7.4. (The ANS-IFABP data have been concentration normalized from 1.95 to 2.12 mM.) The bulk water relaxation rate measured together with the apo-IFABP (□) and holo-IFABP (◆) samples is also shown. The estimated error bars are of the same size as the data symbols. The curves resulted from constrained bi-Lorentzian fits with the parameter values given in Tables 1-3.

plex with the fatty acid anions palmitate (C16:0) and oleate (C18:1 *cis*- Δ 9) and with the anionic fluorescent dye ANS. Measurements have been performed with two protein batches (I and II), at two temperatures (4 °C and 27 °C), and at two pH values (5.7 and 7.4), in total 22 dispersion profiles. Protein batch I contains a polybasic impurity, which does not affect the internal hydration (see Materials and Methods).

Figure 2(a) shows the ¹⁷O dispersions measured at 27 °C on solutions of IFABP in the apo form and in complex with oleate and ANS. Several unexpected conclusions follow directly from these data. (1) The dispersion step from apo-IFABP is small, comparable with that observed with other proteins of similar size, but with only a few internal water molecules (Denisov & Halle, 1996). (2) Although oleate appears to expell 14 of the 22 water molecules in the cavity of apo-IFABP (Sacchettini & Gordon, 1993), the dispersion amplitude increases slightly on oleate binding, implying that the holo-protein has a greater number of long-lived water molecules or, at least, that any reduction of the number of such water molecules is more than compensated by an increased orientational order of the remaining ones. (3) While ANS and oleate have similar van der Waals volumes (227 and 256 Å³,

respectively), they differ greatly in structure and interaction potential. Moreover, ANS binds in a different part of the cavity (Kurian, 1998), displacing a different set of cavity water molecules. Yet, ANS and oleate have virtually the same effect on the ¹⁷O dispersion. The simplest explanation of these three observations is that nearly all water molecules in the cavity of both apo and holo forms are short-lived (i.e. their exchange is faster than the protein tumbling) and therefore, do not contribute significantly to the relaxation dispersion. The dispersion must then be dominated by long-lived water molecules located outside the cavity, where they would not be perturbed by ligand binding.

Figure 2(b) demonstrates that the three qualitative features observed at 27 °C persist at 4 °C. The principal effect of reducing the temperature is a low-frequency shift of all dispersions, as expected from the slower protein tumbling; the rotational correlation time τ_R of the protein is expected to scale as η/T (Table 1). The twofold increase in solvent viscosity is also manifested in the bulk water relaxation rate, $R_{1,\text{bulk}}$ (data points at the bottom of Figure 2), measured together with the protein samples.

The corresponding ²H dispersions, shown in Figure 2(c) and (d), reinforce the ¹⁷O results: the dispersion step is small and ligand binding has little effect. The different ordering of the three closely-spaced ²H dispersion profiles as compared to the ¹⁷O profiles can be explained by even a small contribution to the ²H relaxation rate from labile protein hydrogen atoms in fast exchange with the water hydrogen pool (Denisov & Halle, 1995b; Halle *et al.*, 1999). To assess the importance of labile hydrogen atoms, we measured the ²H and ¹⁷O dispersions for apo-IFABP at pH* 5.7. (All other data were obtained at pH* 7.4.) As seen from Figure 3, this pH shift has little effect on the ²H dispersion, suggesting that the labile hydrogen

Table 1. Temperature dependence of bulk water properties

Property	4 °C	27 °C
¹⁷ O $R_{1,\text{bulk}}$ (s ⁻¹)	307.8(±1.3)	151.0(±0.4)
² H $R_{1,\text{bulk}}$ (s ⁻¹)	4.06(±0.02)	2.00(±0.1)
η (cP)	1.85	0.968
Batch I τ_R (ns)	16.8	8.1
Batch II τ_R (ns)	14.7	7.1

All quantities refer to water with 51.8 at % ²H, 16.9 at % ¹⁷O, and 28.9 at % ¹⁸O.

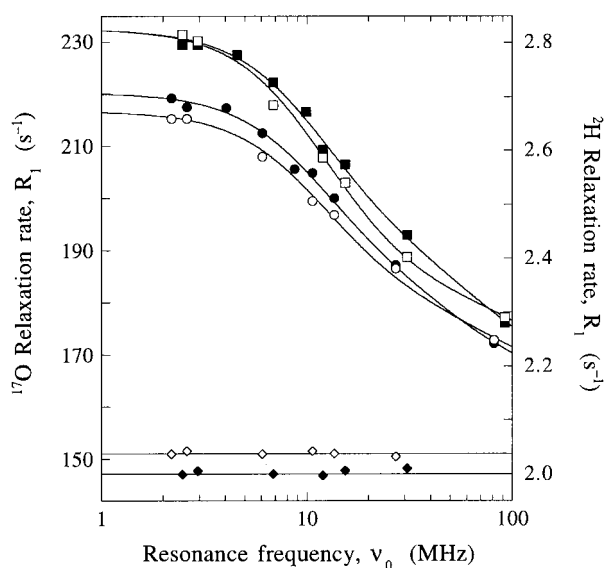


Figure 3. Frequency dependence of water ^{17}O (circles) and ^2H (squares) longitudinal relaxation rates at 27°C in 2.11 mM solutions of apo-IFABP (batch II) at $\text{pH}^* 7.4$ (filled symbols) and $\text{pH}^* 5.7$ (open symbols). (The $\text{pH}^* 5.7$ data have been concentration normalized from 2.49 to 2.11 mM.) The bulk water ^{17}O (\diamond) and ^2H (\blacklozenge) relaxation rates are also shown. The estimated error bars are of the same size as the data symbols. The curves resulted from constrained bi-Lorentzian fits with the parameter values given in Tables 1-3.

contribution is minor. The insignificant effect on the ^{17}O dispersion shows that the long-lived water molecules are unaffected by the pH change, as expected.

In all cases, the dispersion profiles from the apo and holo forms converge at the highest investigated frequency (Figures 2 and 3). The high-frequency plateau of the dispersion profile reflects the dynamic retardation of short-lived water molecules, most of which reside at the protein surface. Since the structure of IFABP changes

very little on fatty acid binding (Sacchettini & Gordon, 1993), the high-frequency plateau should be the same for the apo and holo forms. The dispersion data in Figures 2 and 3, however, provide little direct evidence of a high-frequency plateau. The persistence of the dispersion up to 100 MHz and beyond indicates an important relaxation contribution from motions an order of magnitude faster than protein tumbling. The MRD data therefore cannot be quantitatively described by a single correlation time.

Quantitative analysis of low-frequency dispersion

The need to invoke two correlation times complicates the analysis (see Materials and Methods for details of the data reduction protocol). The bi-Lorentzian function used to analyze the MRD data involves five parameters: α determines the high-frequency plateau (not directly observable), β and τ_β are the amplitude and correlation time of the low-frequency dispersion step, and γ and τ_γ are the corresponding quantities for the high-frequency step.

In the first stage of the analysis, we determined the correlation time τ_β of the low-frequency dispersion step. This can be done most accurately at 27°C , where we obtain $\tau_\beta = 7.1(\pm 0.2)$ ns (batch II), in quantitative agreement with the two previous determinations (Frolov & Schroeder, 1997; Hodsdon & Cistola, 1997b) of the rotational correlation time τ_R of IFABP (after scaling to our temperature and solvent viscosity; see Materials and Methods). In general the observed correlation time τ_β is given by $1/\tau_\beta = 1/\tau_R + 1/\tau_W$ (Halle *et al.*, 1999). The finding that $\tau_\beta = \tau_R$ thus implies that the water molecules responsible for the dispersion have residence times τ_W long compared to τ_R . The identification $\tau_\beta = \tau_R$ is also consistent with the finding that the ^{17}O and ^2H data yield the same τ_β (Halle *et al.*, 1999). Furthermore, we find no significant variation in τ_β between the apo and holo forms. This is consistent with the previous τ_R

Table 2. Results derived from two-parameter constrained Lorentzian fits to low-frequency ^{17}O and ^2H MRD data

Protein	T ($^\circ\text{C}$)	pH^*	$N_\beta S_\beta^2$		$10^{-3} N_\alpha \rho_\alpha + KN_\gamma S_\gamma^2 \tau_\gamma^a$	
			^{17}O	^2H	^{17}O	^2H
Apo(I)	27	7.4	2.1(± 0.1)	3.0(± 0.2)	6.6(± 0.1)	12.0(± 0.5)
Apo(II)	27	7.4	2.4(± 0.2)	2.0(± 0.1)	5.2(± 0.3)	5.0(± 0.2)
Apo(II)	27	5.7	2.4(± 0.2)	2.4(± 0.2)	4.6(± 0.3)	4.1(± 0.4)
C16(II)	27	7.4	3.0(± 0.3)	2.3(± 0.2)	5.1(± 0.5)	4.4(± 0.3)
C18(I)	27	7.4	2.7(± 0.1)	2.6(± 0.2)	6.5(± 0.2)	11.2(± 0.5)
ANS(I)	27	7.4	2.7(± 0.1)	2.8(± 0.2)	7.0(± 0.2)	12.4(± 0.5)
Apo(I)	4	7.4	2.4(± 0.1)	1.5(± 0.2)	9.2(± 0.2)	8.2(± 0.3)
Apo(II)	4	7.4	2.9(± 0.2)	2.0(± 0.2)	6.8(± 0.3)	4.9(± 0.3)
C16(II)	4	7.4	3.3(± 0.2)	2.0(± 0.1)	6.4(± 0.4)	4.8(± 0.1)
C18(I)	4	7.4	2.9(± 0.3)	2.3(± 0.1)	9.0(± 0.5)	7.0(± 0.2)
ANS(I)	4	7.4	2.9(± 0.2)	2.5(± 0.2)	10.2(± 0.3)	7.7(± 0.3)

Fits to data points at frequencies <25 MHz (27°C) or <13 MHz (4°C) with τ_β fixed at the values given in Table 1. Parameter errors were obtained by adjusting the experimental error in the R_1 data (0.2-1.2%) to obtain $\chi^2 \approx 1$.

^a $K = \omega_0^2/R_{1,\text{bulk}} = 0.38 \text{ ns}^{-1}$ (27°C) or 0.19 ns^{-1} (4°C) for both nuclei.

results (Frolov & Schroeder, 1997; Hodsdon & Cistola, 1997b) and with the insignificant effect of ligand binding on crystal structures of IFABP (Sacchettini *et al.*, 1989a, 1992; Scapin *et al.*, 1992; Eads *et al.*, 1993).

To more accurately monitor variations in β on ligand binding, we fix τ_β and determine β from two-parameter Lorentzian fits (see Materials and Methods). The results of these constrained fits are collected in Table 2, where the amplitude parameter β has been converted to the microscopic quantity $N_\beta S_\beta^2 = \beta N_T / \omega_Q^2$, with N_β the number of long-lived ($\tau_W \gg \tau_R$) water molecules and S_β^2 their mean-square orientational order parameter. The overall water/protein molar ratio N_T is obtained from the protein concentration and the rigid-lattice quadrupole frequency ω_Q is $7.61 \times 10^6 \text{ rad s}^{-1}$ for ^{17}O and $8.70 \times 10^5 \text{ rad s}^{-1}$ for ^2H (Halle *et al.*, 1999).

We consider first the $N_\beta S_\beta^2$ values derived from the ^{17}O data. In all cases, the results can be accounted for by as little as three or four water molecules, although this number (N_β) would be larger if the long-lived water molecules were orientationally disordered ($S_\beta^2 \ll 1$). The residence times of the water molecules responsible for the β dispersion must be long compared to τ_R , but short compared to the local zero-frequency spin relaxation time (Halle *et al.*, 1999). The most restrictive bounds are obtained at 4°C , where we require that $0.02 \leq \tau_W \leq 2 \mu\text{s}$ (the upper bound assumes $S_\beta = 0.8$). At both temperatures, ligand binding produces a small but significant increase of $N_\beta S_\beta^2$ by 0.4–0.6 units. There is no significant difference in this respect between the three ligands or between the two temperatures. The oleate and ANS complexes yield identical $N_\beta S_\beta^2$ values (at both temperatures), despite substantial differences in molecular properties and binding mode (see above). The effect of oleate and ANS binding is displayed more clearly in Figure 4, where the two free parameters in a Lorentzian dispersion function with fixed τ_β are fitted to the holo-apo difference data. These direct difference fits yield $\Delta(N_\beta S_\beta^2) = 0.68(\pm 0.05)$ for oleate and $0.60(\pm 0.03)$ for ANS, in agreement with (but more accurate than) the results in Table 3. The holo-apo R_1 difference is seen to be small at higher frequencies, as expected if the γ dispersion and the high-frequency plateau are unaffected by ligand binding.

The $N_\beta S_\beta^2$ values derived from the ^2H data do not differ much from the ^{17}O values, suggesting that they are dominated by long-lived water molecules rather than by labile hydrogen atoms. The effect of ligand binding on $N_\beta S_\beta^2$ is less clearcut than for ^{17}O and suggests a small contribution from hydroxyl, ammonium, and guanidinium deuterons with residence times in the sub-millisecond range (Denisov & Halle, 1995b; Liepinsh & Otting, 1996). The small increase of $N_\beta S_\beta^2$ at $\text{pH}^* 5.7$ presumably reflects the titration of an aspartate or glutamate COOD group with electrostatically up-shifted pK_a value; solvent-exposed carboxylic

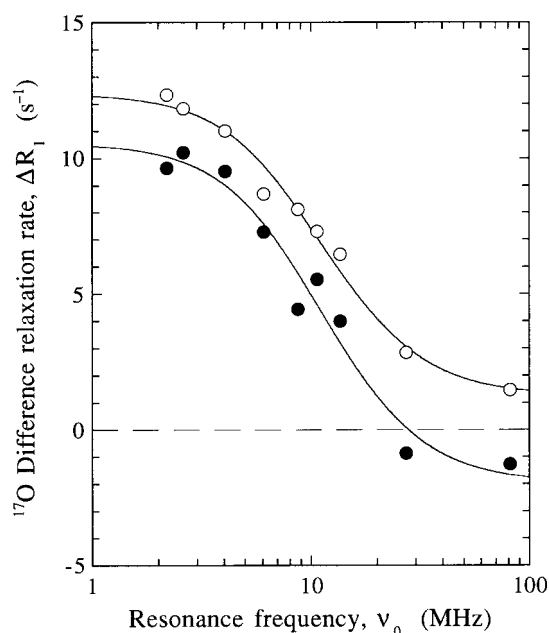


Figure 4. Enhancement of the water ^{17}O longitudinal relaxation rate induced by binding of oleate (●) and ANS (○) to IFABP (batch I) at 2.12 mM, 27°C , and $\text{pH}^* 7.4$. (Before subtraction, the ANS-IFABP data were concentration normalized from 1.95 to 2.12 mM.) The curves resulted from constrained Lorentzian fits with τ_β fixed at 8.1 ns.

hydrogen atoms are invariably in fast exchange with water (Lankhorst *et al.*, 1983). The consistent reduction of $N_\beta S_\beta^2$ at the lower temperature is probably due to slower hydrogen exchange, making the labile hydrogen contribution negligible at 4°C . Since the local ^2H relaxation rate of a long-lived and highly ordered water molecule is about $140 \mu\text{s}$, as compared to $2 \mu\text{s}$ for ^{17}O , water molecules with residence times in the range 2–140 μs (at 4°C) would only contribute to the ^2H dispersion. The finding that $N_\beta S_\beta^2$ is smaller for ^2H therefore suggests that such water molecules are not present in IFABP. Local reorientation of long-lived water molecules during their residence time reduces the ^2H and ^{17}O order parameters to different extent (Halle *et al.*, 1999). In particular, a symmetric 180° flip of an otherwise ordered water molecule reduces $S_\beta^2(\text{H})$ from 1 to 0.37, but has no effect on $S_\beta^2(^{17}\text{O})$. The ratio $S_\beta^2(^2\text{H})/S_\beta^2(^{17}\text{O}) = 0.7(\pm 0.1)$ observed at 4°C therefore suggests that some, but not all, of the long-lived water molecules have flip times shorter than the protein tumbling time (15 ns at 4°C).

Quantitative analysis of high-frequency dispersion

The effective α parameter determined from constrained Lorentzian fits to low-frequency data (in the region of the β dispersion) incorporates the low-frequency limit of the γ contribution, and can

Table 3. Results derived from two-parameter constrained bi-Lorentzian fits to complete ^{17}O and ^2H MRD data

Protein	T ($^{\circ}\text{C}$)	pH*	$10^{-3} N_{\alpha}\rho_{\alpha}$		$N_{\gamma}S_{\gamma}^2$		τ_{γ} (ns)	
			^{17}O	^2H	^{17}O	^2H	^{17}O	^2H
Apo(I)	27	7.4	[3.6]	[7.3]	7.1(\pm 0.4)	8(\pm 2)	1.1(\pm 0.1)	1.6(\pm 0.4)
Apo(II)	27	7.4	[2.1]	[2.1]	6.2(\pm 0.7)	7.3(\pm 0.8)	1.3(\pm 0.2)	1.1(\pm 0.1)
Apo(II)	27	5.7	[2.1]	[2.1]	7(\pm 2)	9(\pm 2)	0.9(\pm 0.2)	0.6(\pm 0.2)
C16(II)	27	7.4	[2.1]	[2.1]	8(\pm 2)	13(\pm 0.4)	0.9(\pm 0.2)	0.5(\pm 0.2)
C18(I)	27	7.4	[3.6]	[7.3]	5.7(\pm 0.6)	7(\pm 2)	1.3(\pm 0.2)	1.6(\pm 0.4)
ANS(I)	27	7.4	[3.6]	[7.3]	8.0(\pm 0.7)	10(\pm 2)	1.1(\pm 0.1)	1.4(\pm 0.3)
Apo(I)	4	7.4	[4.8]	[4.8]	7.4(\pm 0.8)	6.2(\pm 0.7)	3.3(\pm 0.4)	3.0(\pm 0.2)
Apo(II)	4	7.4	[2.6]	[2.6]	7.8(\pm 0.8)	5.6(\pm 0.8)	2.9(\pm 0.4)	2.3(\pm 0.4)
C16(II)	4	7.4	[2.6]	[2.6]	8(\pm 1)	7(\pm 3)	2.5(\pm 0.4)	1.6(\pm 0.6)
C18(I)	4	7.4	[4.8]	[4.8]	7(\pm 1)	5(\pm 1)	3.2(\pm 0.6)	2.5(\pm 0.6)
ANS(I)	4	7.4	[4.8]	[4.8]	9(\pm 1)	7(\pm 1)	3.2(\pm 0.4)	2.3(\pm 0.4)

Fits to all data, with τ_{β} and $N_{\beta}S_{\beta}^2$ fixed at values in Tables 1 and 2 and $N_{\alpha}\rho_{\alpha}$ fixed at values in square brackets. Parameter errors were obtained by adjusting the experimental error in the R_1 data (0.2-1.5%) to obtain $\chi^2 \approx 1$.

therefore be expressed as $\alpha + \gamma \tau_{\gamma}$. The true α parameter can usually be accounted for by short-lived water molecules in contact with the protein surface, rotating (on average) about fivefold slower than in bulk water (Denisov & Halle, 1996). The parameter α can be converted to the microscopic quantity $N_{\alpha}\rho_{\alpha} = \alpha N_T / R_{1,\text{bulk}}$, with N_{α} the number of surface water molecules and $\rho_{\alpha} = (\tau_{\alpha} / \tau_{\text{bulk}} - 1)$ their average relative dynamic retardation. The N_{α} value can be estimated from the (external) solvent-accessible surface area (calculated with a probe radius of 1.4 Å), 6930 Å² for IFABP (with negligible difference between the apo and holo forms), and dividing by the mean surface area occupied by a water molecule at the surface, taken as 15 Å². This yields $N_{\alpha} = 460$ for IFABP. If the composite parameter $\alpha + \gamma \tau_{\gamma}$ (or its microscopic equivalent, given in Table 2) were interpreted as the true α parameter (i.e. neglecting the γ dispersion), then ρ_{α} would become more than twice as large as the values of 4-5 obtained for nearly all globular proteins so far investigated. Such large (apparent) dynamic retardation factors have only been obtained for carbonic anhydrase (Denisov *et al.*, 1999), trypsin, and serum albumin (Denisov & Halle, 1996), all of which contain large numbers of buried water molecules, some of which occur in clusters. We therefore attribute the γ dispersion in IFABP to the large water cluster in the binding cavity.

To further characterize the γ dispersion, we made use of the high-frequency R_1 data that were omitted in the Lorentzian fits to data in the β dispersion region. We thus performed constrained bi-Lorentzian fits with τ_{β} and N_{β} fixed at the values determined from the low-frequency data and $N_{\alpha}\rho_{\alpha}$ fixed at the expected value $460 \times 4.5 = 2100$ for ^{17}O at 27°C (see Materials and Methods). The resulting values of the two newly adjusted parameters, γ and τ_{γ} , are given in Table 3. For all samples and for both nuclei, τ_{γ} is about 1 ns (mean 1.1 ns) at 27°C, increasing to about 3 ns (mean 2.7 ns) at 4°C. The quantity $N_{\gamma}S_{\gamma}^2$ is 7(\pm 2) in all cases, but is less reliably determined than τ_{γ} , since it couples with $N_{\alpha}\rho_{\alpha}$ and therefore depends on the

assumptions made about $N_{\alpha}\rho_{\alpha}$. Nevertheless, we can conclude that $N_{\gamma}S_{\gamma}^2$ does not vary greatly between the apo and holo forms or between 4°C and 27°C, and that the γ dispersion is due to at least half a dozen, and probably more, water molecules.

To emphasize the anomalous γ dispersion seen in all our MRD profiles, Figure 5 compares the ^{17}O

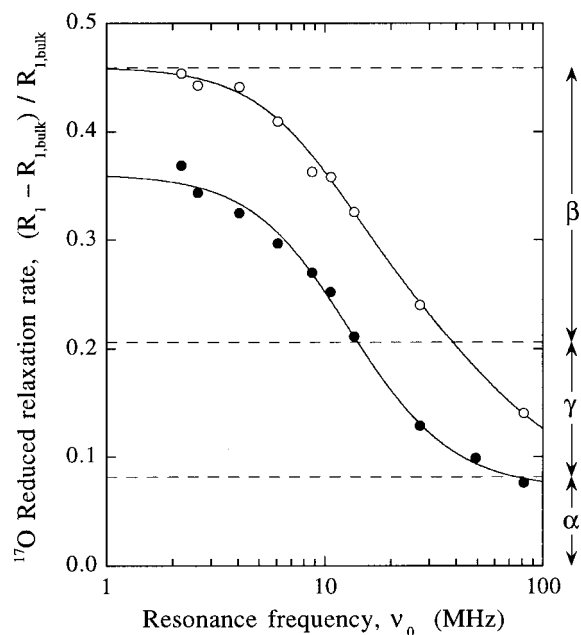


Figure 5. Frequency dependence of water ^{17}O longitudinal relaxation rate in aqueous solutions of 2.1 mM apo-IFABP (batch II), pH* 7.4 (O) and 1.9 mM bovine α -lactalbumin, pH* 8.4 (●), both at 27°C. The measured R_1 values have been normalized by the bulk water relaxation rate $R_{1,\text{bulk}}$ to remove the effect of the isotope composition of the water. In addition, the α -lactalbumin data have been concentration normalized to the same water/protein mole ratio as for IFABP. The regions between the dashed lines correspond to the α , β , and γ contributions to R_1 in the low-frequency limit. The α -lactalbumin data are taken from (Denisov *et al.*, 1999) and the curve is a Lorentzian fit.

dispersion profile from apo-IFABP with the more typical profile from bovine α -lactalbumin (BLA; Denisov *et al.*, 1999). BLA does not differ much from IFABP with regard to size (14.2 kDa, $N_\alpha = 470$, $\tau_R = 6.9$ ns) or low-frequency dispersion step ($N_\beta S_\beta^2 = 3.2$). The BLA dispersion, however, does not exhibit the strong frequency dependence seen for IFABP above 20 MHz and is well described by a Lorentzian dispersion function.

Discussion

Identification of long-lived water molecules

On the basis of the MRD results in Tables 2 and 3, we can categorically rule out the possibility that the 14 displaced water molecules are long-lived ($\tau_W > 10$ ns) and highly ordered. The small increase, by 0.4-0.7 units, in $N_\beta S_\beta^2$ on ligand binding could, in principle, result from nearly compensating changes in N_β and S_β^2 , e.g. a decrease in N_β from 22 to eight accompanied by a threefold increase in S_β^2 due to further ordering of the remaining water molecules. This scenario can be rejected on two grounds. First, the eight conserved water molecules are extensively H-bonded to the protein and to each other in both apo and holo forms and should, therefore, not be very much perturbed by the fatty acid. Second, $N_\beta S_\beta^2$ is nearly the same for the ANS and fatty acid complexes, although these ligands displace different water molecules and interact differently with the remaining ones. We therefore conclude that the dispersions are produced by a small number of water molecules, most of which are conserved between the apo and holo forms.

Although the location of the long-lived water molecules cannot be determined from the MRD data, plausible assignments can be made to crystallographically identified hydration sites. We thus analyzed crystal structures of apo and holo-IFABP in terms of three structural indicators that are correlated with the residence time of hydration water molecules (Denisov & Halle, 1996): their solvent accessible surface area (A_S), crystallographic B -factor, and hydrogen-bonding status. Fully buried water molecules ($A_S = 0$) typically have B -factors in the range 10-15 \AA^2 and three or four H-bonds to the protein. Water molecules residing in surface pockets or crevices, although slightly exposed ($A_S < 10 \text{\AA}^2$), can also be long-lived and then usually have $B < 20 \text{\AA}^2$ and at least three H-bonds to the protein. In applying these "ABH criteria" to the crystallographic data, we added hydrogen atoms to the PDB files and calculated A_S with the program GRASP (Nicholls *et al.*, 1993) using a probe radius of 1.4 \AA (yielding $A_S = 113 \text{\AA}^2$ for a fully exposed water molecule).

We consider first the possibility that some of the long-lived water molecules contributing to the β dispersion of both apo and holo-IFABP are located in the binding cavity. Among the eight water molecules that are conserved in the holo-protein, at

most two or three can be long-lived according to the ABH criteria (Table 4). (We consider here the residence time in the crystallographic hydration site. This site residence time may well be considerably shorter than the residence time in the cavity, at least for water molecules that do not satisfy the ABH criteria.) Among these, W137 is without doubt the best candidate. It resides in a pocket in the cavity wall just inside the portal, makes three strong H-bonds to the protein, and has the smallest B -factor among all cavity waters in every (apo and holo) crystal structure. Outside the cavity, we find five potentially long-lived water molecules that satisfy the ABH criteria (Table 4). Prominent among these is W135, which is buried ($A_S = 0$) in a small cavity in the upper part of the gap region, apparently playing a critical structural role by connecting the loop between β -strands D and E *via* strong H-bonds to strand F in the orthogonal β -sheet (Figure 1). This internal water molecule is conserved in other members of the iLBP family (Banaszak *et al.*, 1994), makes three strong H-bonds to the protein backbone, and has the smallest B -factor among all the 238 water molecules in the apo-IFABP structure.

The β dispersion from apo-IFABP can be accounted for by three highly ordered and long-lived water molecules. The crystal structure analysis (Table 4) suggests a parsimonious set of long-lived water molecules: W137 in the cavity, and W135 and W217 outside the cavity. Since these three water molecules are conserved in all holo-IFABP structures, they should contribute to the β dispersions from the palmitate and oleate complexes investigated here. The solution structure of the ANS-IFABP complex (Kurian, 1998) suggests that these three water molecules are also conserved in the ANS complex.

The increase of $N_\beta S_\beta^2$ by 0.4-0.7 units on fatty acid and ANS binding can be explained by one ordered water molecule that becomes long-lived as a result of ligand binding. The increased residence time could be due to a strong electrostatic interaction with the ligand (fatty acid carboxylate or ANS sulfonate group) or it might result from trapping of one or more water molecules in an intracavity pocket sealed off by the ligand. A possible candidate for the former scenario is W147, which is probably short-lived in apo-IFABP, but may become long-lived through the additional H-bond to one of the carboxylate oxygen atoms in the fatty acid headgroup (Table 4). This hypothesis is supported by a ^{19}F -detected heteronuclear NOE study of IFABP complexed with [2-mono- ^{19}F]-palmitate (Cistola & Hall, 1995), indicating that W37 (which corresponds to W170 in the myristate-IFABP complex and to W147 in apo-IFABP, see Table 4) is long-lived in the holo-protein. The finding that ANS has virtually the same effect on $N_\beta S_\beta^2$ as oleate would then suggest a similar explanation for the ANS complex, presumably involving a water molecule that mediates a H-bond between the sulfo-

Table 4. Potentially long-lived water molecules conserved in apo, myristate, and oleate-IFABP

Apo	Water ^a		B (Å ²) ^b			A _S (Å ²) ^c	H-bond ^d	R _{OX} (Å)			NOE ^e	R _{HH} (Å) ^f		
	C14	C18	Apo	C14	C18			Apo	C14	C18				
135	134	222	10.0	15.9	14.4	0.0	Glu63:O	2.8	2.9	2.8	Val66	2.4; 2.6		
							Val66:O	2.9	2.8	2.8			Trp82	2.7; 2.7
							Trp82:N	2.9	3.0	3.0			Gly65	3.2; 3.8
136	167	167	22.3	18.4	23.4	C	Tyr117:O ⁿ	3.0	2.9	3.2	None			
							Arg126:N ⁿ	3.0	3.1	3.0				
							Tyr14:O ⁿ	3.1	3.0	3.2				
137	183	183	13.4	13.1	14.0	C	Tyr14:O ⁿ	2.6	2.8	2.7	None			
							Gly31:O	2.9	3.0	2.9				
							Asp34:O ^δ	3.0	3.0	2.8				
147	170	37 ^g	31.5	28.7	14.0 ^g	C	Glu51:O ^ε	2.4	2.8	2.7 ^g	None			
							FA:O	3.0 ^h	2.8 ⁱ	3.2 ^{g,i}				
152	184	184	14.3	31.1	24.1	C	Ser53:O ^γ	2.9	2.8	2.8	None			
							Glu51:O ^ε	3.0	2.7	2.6				
197	149	148	15.2	15.4	21.6	3.0-6.3	Thr41:O ^γ	2.9	3.2	3.2	Lys50	2.9; 3.4		
							Thr39:O	3.1	3.0	3.1				
							Thr48:O	3.2	3.2	3.1				
215	157	155	17.5	21.9	24.4	1.2-4.4	Val90:O	2.9	3.1	3.2	Lys92	2.4; 3.0		
							Thr81:O ^γ	3.0	3.1	2.9				
							Thr83:O ^γ	3.1	3.1	3.2				
							Thr81:O	3.2	3.0	3.2				
217	158	156	11.5	16.0	18.4	0.4-0.5	Glu107:O ^ε	2.6	2.8	2.8	Glu107	3.0; 3.8		
							Thr116:O ^γ	2.6	2.8	2.5				
							Ile114:O	2.8	3.0	3.3				
							Val105:O	3.2	3.2	3.3				
268	173	214	20.0	31.7	28.5	4.4-7.0	Glu77:O	2.7	3.0	2.7	Val96	2.0 (2.6)		
							Asp97:N	3.2	2.6	2.6			Asp97	2.4 (1.8)
							Val96:N	3.1	3.1	3.0				
							Asp97:O ^δ	3.2	2.7	3.2				

Crystal structures analyzed: apo-IFABP (PDB code 1lfc, 1.2 Å resolution), myristate-IFABP (1icm, 1.5 Å), and oleate-IFABP(R106Q) (1icn, 1.75 Å).

^a Waters in bold-face are assigned to the β dispersion.

^b Isotropic Debye-Waller factor for water oxygen.

^c Solvent-accessible surface area. C denotes water in the binding cavity.

^d Conserved H-bonds with water O-protein O/N separation <3.5 Å.

^e Predicted peptide NH-water NOEs; observed NOEs in bold-face.

^f Peptide NH-water H separations. Water protons were placed with linear H-bonds and 0.98 Å O-H bond length. Where the water orientation was ambiguous, the NH-O distance is given in parentheses.

^g Entry refers to the palmitate-IFABP complex (2ifb, 1.9 Å).

^h H-bond to Arg106:Nⁿ, present only in apo-form.

ⁱ H-bond to fatty acid carboxylate oxygen.

nate group of ANS and the guanidinium group of Arg126 (Kurian, 1998).

We now consider the γ dispersion, with $N_{\gamma}S_{\gamma}^2$ in the range 6-9 and a correlation time $\tau_{\gamma} \approx 1$ ns at 27 °C. Since these water molecules should be less ordered than the more long-lived β water molecules, we estimate their number (N_{γ}) to be 10-20. While a few water molecules in surface pockets may contribute to the γ dispersion (e.g. the four external water molecules in Table 4 that were not assigned to the β dispersion), these can hardly account for the large γ dispersion amplitude. Moreover, since the γ dispersion is only seen for proteins with large internal water clusters, it is presumably related to the binding cavity of IFABP.

While only eight cavity water molecules have been identified in holo-IFABP, the large size of the cavity suggests that not all buried water molecules are crystallographically visible. A cavity search, using the program GRASP (Nicholls *et al.*, 1993) with a probe radius of 1.2 Å (Hubbard & Argos, 1995), on the crystal structure of the myristate complex (PDB code 1icm) revealed three large cavities (59, 68, and 87 Å³) apart from the 361 Å³ cavity

containing the eight crystallographically identified water molecules (Figure 6). The “new” cavities may contain water molecules that are not sufficiently (positionally) ordered or are not present at sufficiently high occupancy to be visible in the electron density map. Such X-ray invisible cavity waters have previously been identified by NOEs in interleukin-1β (Ernst *et al.*, 1995) and lysozyme (Otting *et al.*, 1997) and inferred from MRD data in myoglobin (Denisov & Halle, 1996). In this connection, it is noteworthy that the number of identified cavity water molecules in apo-IFABP increased from 13 at 1.96 Å resolution (Sacchettini *et al.*, 1989b) to 22 at 1.19 Å resolution (Scapin *et al.*, 1992). Interestingly, we find that the total cavity volume (after removal of fatty acid and cavity water molecules) is 40% larger in holo-IFABP (1058 and 1107 Å³, respectively, for the myristate and oleate complexes) than in apo-IFABP (760 Å³).

The correlation time τ_{γ} reflects molecular motions that randomize the orientation of the 10-20 cavity water molecules that we associate with the γ dispersion. Reorientational motions in intact

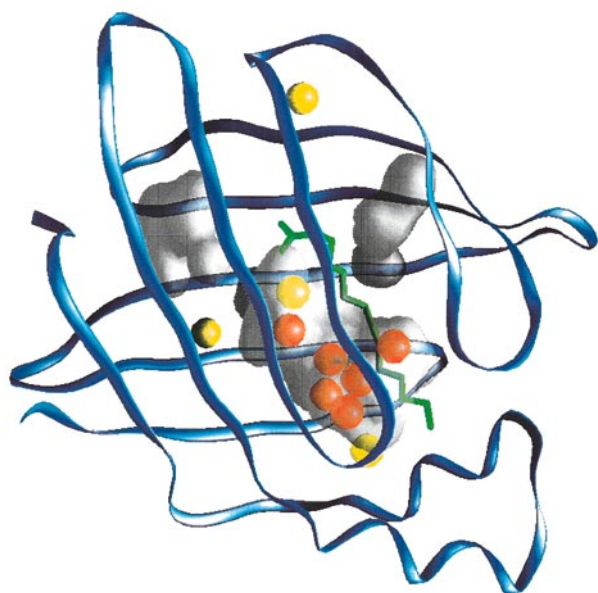


Figure 6. Crystal structure (PDB code 1icm) of holo-IFABP (blue ribbon) with bound myristate (green) showing the four water molecules (yellow) assigned to the β dispersion of holo-IFABP (from top to bottom: W134, W170, W158, and W183; see Table 4 for correspondence to apo water molecules). The six remaining crystallographically identified cavity waters (red) appear to be more short-lived. Four internal cavities detected by a 1.2 Å probe are also shown.

hydration sites within the cavity would be much faster than 1 ns (librations within the H-bond network) or would not affect the ^{17}O relaxation for symmetry reasons (180° flips). The γ dispersion therefore requires that water molecules exchange among hydration sites (with different orientations) and/or that they escape from the cavity. In either case, water translation is probably coupled to protein conformational changes.

Comparison with other studies of FABP hydration in solution

An ^{15}N -edited water-NOE study of IFABP in complex with ANS has recently been performed at 30°C (V.A.L., N.J., S.M. & F.G.P., unpublished results). Only two cross-peaks (with positive intensity in the NOESY spectrum) were observed that can be attributed to long-lived ($\tau_w > 0.3$ ns) water molecules. These involved the peptide NH protons of Va166 and Thr76, and can be explained by a single long-lived water molecule (W135). While this finding is in line with our crystallographically based assignment of W135 as a contributor to the β dispersion, the MRD results demonstrate that there are at least two additional long-lived ($\tau_w \gg 7$ ns) water molecules and probably 10-20 water molecules with a correlation time of about 1 ns, all of which could produce positive NOESY cross-peaks.

To ascertain whether the MRD and NOE results are mutually consistent, we assessed the NOE-observability of individual water molecules by extracting the relevant NH-HOH and NH-(labile H) separations from the 1.2 Å crystal structure of apo-IFABP (PDB code 1icf). Hydrogen atoms were added to the protein and, when two H-bond acceptors could be identified, also to water oxygen atoms (assuming linear H-bonds). This analysis showed that among the 22 crystallographically identified cavity waters in apo-IFABP, only five are NOE-observable: W138 (water oxygen 3.2 Å from peptide NH proton of Arg126), W141 (Ala73, 1.8 Å), W143 (Asp74, 2.8 Å), W149 (Gly31, 3.7 Å), and W156 (Gln 115, 3.6 Å). On the basis of the ABH criteria, all of these water molecules are expected to be short-lived and would therefore probably not produce detectable cross-peaks. The remaining 17 cavity water molecules are either more than 5 Å from any peptide NH proton or contribute slightly to cross-peaks that are strongly (>80%) dominated by dipole couplings to other water molecules or to labile protons. In particular, none of the four potentially long-lived cavity water molecules included in Table 4 are NOE-observable. The absence of cross-peaks with cavity water molecules in the NOE study of the ANS-IFABP complex is therefore consistent with the MRD results, as well as with the crystallographic data.

All five potentially long-lived external water molecules in apo-IFABP are NOE-observable (Table 4). The cross-peaks predicted for these water molecules have negligible contributions from other waters or from labile protons. In the ANS-IFABP NOE study, only cross-peaks with W135 were observed. The absence of the other predicted cross-peaks may imply short residence times for these waters, but could also be due to spectral overlap. If our interpretation of the γ dispersion is correct, the 10-20 γ water molecules with residence times of about 1 ns (controlled by cavity fluctuations) are not expected to be NOE-observable, since the correlation time is short and since most of them are remote from peptide NH protons (see above). We therefore conclude that there is no obvious inconsistency between the NOE and MRD results.

A ^{15}N -edited water-NOE study has been reported for bovine HFABP at 37°C (Mesgarzadeh *et al.*, 1998). For holo-HFABP (with a mixture of endogenous fatty acids), 21 NOEs were attributed to long-lived ($\tau_w > 0.3$ ns) water molecules, as compared to two in the ANS-IFABP complex (V.A.L., N.J., S.M. & F.G.P., unpublished results). Considering that HFABP and IFABP have similar backbone folds, with 1.4 Å C^α RMSD (Banaszak *et al.*, 1994), this difference is striking and prompted us to carry out an analysis of NOE-observability for HFABP using the same procedure as for IFABP. On the basis of the 1.4 Å crystal structure of human HFABP complexed with oleate (Young *et al.*, 1994) and the ABH criteria, we expect W166 (corresponding to W135 in apo-IFABP) and W167 (in

the cavity) to be long-lived and NOE observable. (Only 14 of 132 residues differ between human and bovine HFABP and most of these substitutions conserve the polar/non-polar character of the side-chains.) These two water molecules can account for four of the 21 reported NOEs. The remaining NOEs can probably be attributed to a few long-lived water molecules in surface pockets, to proton exchange relayed magnetization transfer, and to demagnetizing field effects (Sobol *et al.*, 1998). The NOE data are, therefore, consistent with a similar small number of long-lived cavity waters in HFABP and IFABP.

Molecular dynamics (MD) simulations can provide details about cavity hydration dynamics that are not readily accessible by experiment. While MD simulations of FABPs have so far focused on the bound fatty acid, some information about the mobility of cavity water has been obtained. Simulations of the hydrated holo-FABPs from heart and adipocyte thus showed that some water molecules remained in the cavity, whereas others escaped during the 1 ns trajectory (Woolf, 1998; Woolf & Tychko, 1998). While the published data do not allow hydration site or cavity residence times to be estimated, they are qualitatively consistent with the present MRD results and with the NOE results discussed above. In particular, none of the cavity waters remain within 4 Å of the fatty acid during the full 1 ns trajectory. A recent 0.8 ns MD simulation of fully hydrated apo-IFABP revealed a large-scale sub-nanosecond motion of β -strands E and F with a concomitant opening of the portal (V. A. Likić & F.G.P., unpublished results). Conformational fluctuations of this type may be responsible for the γ dispersion observed here. Like the present MRD study, the MD simulation (V. A. Likić & F.G.P. unpublished results) indicates a residence time of about 1 ns for the majority of the water molecules in the binding cavity of apo-IFABP.

Materials and Methods

Expression and purification of apo-IFABP

Recombinant apo-IFABP was expressed and purified as described (Kurian 1998). Two batches of IFABP were prepared for this study. For batch I, the anion exchanger was DEAE Sephadex (Sigma Chemicals, MO) washed repeatedly with 1 M HCl and 1 M NaOH, packed into a 5 cm \times 1 cm column, and equilibrated with 50 mM Tris-HCl (pH 8.3). The purity of batch I was assessed by SDS-PAGE, showing no additional bands on the gel. Subsequently, this preparation was found to contain a polybasic impurity (see below). For batch II, a prepacked anion exchange column (Pharmacia Hi Trap Q) was used after extensive washing with 50 mM Tris-HCl (pH 8.3). The purity of batch II was verified by SDS-PAGE, amino acid analysis, and mass spectrometry. For both batches, the purified protein was dialyzed against 20 mM potassium phosphate at pH 5.5, concentrated to ca. 2 mM, and lyophilized.

Preparation of MRD samples

For each MRD sample, ca. 30 mg lyophilized apo-IFABP was dissolved in 1 ml ^2H and ^{17}O -enriched water (52 at% ^2H , 17 at% ^{17}O) obtained from Cambridge Isotope Laboratories (Andover, MA, USA). A small fraction of insoluble protein was removed by centrifugation. The protein was studied at pH* 7.4 and 5.7, adjusted by minute additions of 2 M KOH and 3 M HCl. Quoted pH* values are uncorrected for solvent isotope effects. All samples contained 20 mM potassium phosphate buffer and 0.02 wt% sodium azide. To avoid detergent contamination, only new NMR tubes were used. The protein concentration, determined by complete amino acid analysis (carried out at BMC, Uppsala University, Sweden) after completion of the MRD measurements, was 2.12 mM (batch I) or 2.11 mM (batch II) in all cases, except for the pH* 5.7 sample (2.49 mM) and the ANS complex (1.95 mM).

IFABP from two different protein batches, denoted I and II, was used for the MRD measurements. Amino acid analysis and mass spectrometry showed that batch I contained an impurity, presumably originating from the anion-exchange column used in the last step of the purification protocol (see above). A second batch of IFABP was therefore prepared using a column from a different manufacturer. No impurities were detected in batch II. Comparison of the MRD data from the two batches showed that the impurity affects the dispersion profile in two ways: (1) the direct effect of impurity hydration adds to the frequency-independent "background" relaxation rate of the solvent, and (2) the enhanced viscosity (and/or direct interactions) retards protein tumbling slightly. Since neither ligand binding nor long-lived hydration were affected by the impurity, results from both protein batches are presented and analyzed.

For preparation of holo-IFABP with bound fatty acid, palmitic acid (Sigma P5585, 99%) or oleic acid (Sigma O1008, 99%) was dissolved in chloroform and transferred to a reactival. The solvent was evaporated under a stream of argon gas, leaving the fatty acid coating the glass surface. The apo-IFABP solution was then added and gently stirred for 36-48 hours at 4 °C. The fatty acid to IFABP mole ratio was 1.0 (batch I) or 1.1 (batch II) based on the weighed amount of fatty acid and the protein concentration as determined by amino acid analysis. For preparation of holo-IFABP with bound ANS (from Fluka, Milwaukee, WI), ca. 20 μl of a 100 mM aqueous ANS solution were slowly added to the apo-IFABP solution, which was then gently stirred for 48 hours at 4 °C. The ANS to IFABP mole ratio was 1.1.

Magnetic relaxation measurements

The longitudinal relaxation rate, $R_1 = 1/T_1$, of the water ^{17}O and ^2H resonances in IFABP solutions was measured at up to nine magnetic field strengths in the range 0.38-14.1 T, corresponding to resonance frequencies in the range 2.2-81.3 MHz (^{17}O) and 2.5-92.1 MHz (^2H). The measurements were performed with a Varian 600 Unity Plus spectrometer, Bruker Avance DMX 200 and DMX 100 spectrometers, and a field-variable (0.38-1.83 T) iron magnet (Drusch EAR-35N) equipped with field-variable lock and flux stabilizer and interfaced to a Bruker MSL 100 console. R_1 was measured by the inversion recovery method, using the protocol described (Denisov & Halle, 1995a).

The sample temperature was controlled to within ± 0.1 deg. C by a thermostated flow of air and was checked after each R_1 measurement with a calibrated thermocouple. Most measurements on protein samples were immediately followed by a control measurement on a bulk water reference sample of the same water isotope composition and pH* as in the protein solution. Since the reference R_1 value, denoted $R_{1,\text{bulk}}$, is known to be independent of frequency, it provides an additional check on temperature stability. The (mean) $R_{1,\text{bulk}}$ values are given in Table 1.

MRD data reduction

Relaxation theory

Under the conditions of the present study, the (excess) longitudinal relaxation rate of the quadrupolar ^{17}O and ^2H nuclei can be expressed as (Abragam, 1961; Halle & Wennerström, 1981):

$$R_1 - R_{1,\text{bulk}} = 0.2J(\omega_0) + 0.8J(2\omega_0) \quad (1)$$

where $\omega_0 = 2\pi\nu_0$ is the variable (angular) resonance frequency and $J(\omega)$ is the spectral density function. Water ^{17}O and ^2H MRD profiles from protein solutions can usually be accurately modeled by a Lorentzian spectral density function (plus a constant term; Halle *et al.*, 1999):

$$J(\omega) = \alpha + \beta\tau_\beta[1 + (\omega\tau_\beta)^2]^{-1} \quad (2)$$

where α is the excess relaxation rate on the high-frequency plateau of the dispersion profile and $\beta\tau_\beta$ is the magnitude of the dispersion step. The microscopic significance of the amplitude parameters α and β has been established in previous studies of aqueous protein solutions (Denisov & Halle, 1996). For the present MRD data, the Lorentzian function (2) turned out to be inadequate. The dispersion data were therefore analyzed with the bi-Lorentzian spectral density function:

$$J(\omega) = \alpha + \beta\tau_\beta[1 + (\omega\tau_\beta)^2]^{-1} + \gamma\tau_\gamma[1 + (\omega\tau_\gamma)^2]^{-1} \quad (3)$$

Figure 7 compares Lorentzian and bi-Lorentzian fits to ^{17}O dispersion data from apo-IFABP at 4°C. Here, as elsewhere in this work, non-linear fits were performed with the Levenberg-Marquardt algorithm (Press *et al.*, 1986). The residuals of the three-parameter Lorentzian fit show a systematic frequency variation with deviations of up to 2%, substantially more than the estimated experimental error of 0.5% (based on reproducibility tests). As expected, the five-parameter bi-Lorentzian fit is much better, especially in the high-frequency region where the fit places the γ dispersion. The reduced χ^2 merit function drops from 7.4 for the Lorentzian fit to 0.58 for the bi-Lorentzian fit ($\chi^2 \approx 1$ is expected if the model is correct and the random error is properly assigned). If the measurement errors are normally distributed, the probability of observing a larger relative reduction of χ^2 is merely 1.5%. According to the F test (Press *et al.*, 1986), the two additional parameters in the bi-Lorentzian function are therefore justified by the data. This is the case also for the other ^{17}O and ^2H dispersions measured at 4 and 27°C, which all display the same systematic deviation from Lorentzian shape.

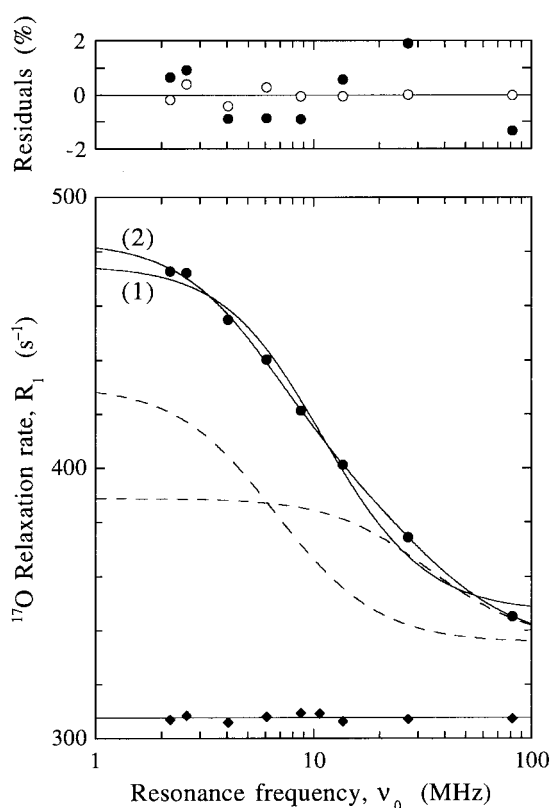


Figure 7. Frequency dependence of water ^{17}O longitudinal relaxation rate (\bullet) from a 2.11 mM solution of apo-IFABP (batch II) at 4°C. The bulk water relaxation rate (\blacklozenge) is also shown. The estimated error bars are of the same size as the data symbols. The continuous curves resulted from Lorentzian (1) and bi-Lorentzian (2) fits. The dashed curves are the individual components of the bi-Lorentzian dispersion. The upper panel shows the residuals from the Lorentzian (\bullet) and bi-Lorentzian (\circ) fits.

Rotational correlation time of IFABP

The conclusion from the preceding statistical analysis is reinforced by an examination of the parameter values resulting from the fits, especially the correlation time τ_β . This parameter is expected to report on the rotational diffusion of the protein, i.e. $\tau_\beta = \tau_R$ (see below). The rotational correlation time of apo-IFABP has been determined to $\tau_R = 6.7$ ns by ^{15}N relaxation under conditions (2 mM protein in 10/90% $^2\text{H}_2\text{O}/\text{H}_2\text{O}$, 20 mM phosphate buffer, 50 mM KCl, pH 7.2, 25°C) similar to ours (Hodsdon & Cistola, 1997b). Assuming that τ_R is proportional to η/T (as predicted by hydrodynamics), we obtain $\tau_R = 7.1$ ns for our conditions. A time-resolved fluorescence anisotropy study of apo-IFABP (2 μM protein in H_2O , 25 mM phosphate buffer, pH 7.4, 25°C) gave $\tau_R = 6.6(\pm 0.2)$ ns (Frolov & Schroeder, 1997), also corresponding to $\tau_R = 7.1$ ns for our conditions. Scaling this value with η/T , we obtain $\tau_R = 14.7$ ns at 4°C (see Table 2). The bi-Lorentzian fit in Figure 7 yields $\tau_\beta = 13.5(\pm 2.5)$ ns, in agreement with the independently determined τ_R , whereas the Lorentzian fit yields $\tau_\beta = 8.7(\pm 0.8)$ ns, much smaller than τ_R at 4°C. Averaged over all dispersions (apo and holo forms, batches I and II,

^{17}O and ^2H), the τ_β values resulting from Lorentzian fits are 9.0 ns at 4 °C and 5.8 ns at 27 °C. The ratio of these values is 1.5, whereas the corresponding τ_R ratio should be 2.1 (see Table 1).

While the Lorentzian spectral density function yields fits of poor quality with systematically distorted parameter values, the bi-Lorentzian function does not allow accurate parameter estimation (due to large covariances between some of the parameters). To overcome this problem, the following strategy was adopted for analyzing the dispersion data at 4 °C and 27 °C. First, the parameters β and τ_β were determined from Lorentzian fits to data in the low-frequency region, where the γ contribution is independent of frequency (cf. the dashed curves in Figure 7). The average τ_β was 7.1(\pm 0.3) ns for batch II, in agreement with the literature values (see above). A slightly larger value, $\tau_\beta = 8.1(\pm 0.3)$ ns, was obtained for batch I. This difference can be attributed to the impurity in batch I (see above), which may increase the hydrodynamic volume of the protein (if it binds to the surface) and/or increase the effective solvent viscosity.

Low-frequency dispersion

In the next step of the analysis, we assumed that $\tau_\beta = \tau_R$, $\tau_R(\text{apo}) = \tau_R(\text{holo})$, as indicated by the MRD data and by earlier studies. By introducing these constraints in the fits, variations in the remaining parameters (β , in particular) on ligand binding and between the two nuclei can be monitored more accurately. At 27 °C we thus fix τ_β to 8.1 ns (batch I) or 7.1 ns (batch II), and at 4 °C the fixed τ_β is obtained from these values by scaling with η/T (Table 1). We then determined β from Lorentzian fits (with two free parameters) to dispersion data in the low-frequency region (<25 MHz at 27 °C and <13 MHz at 4 °C). Since a Lorentzian dispersion depends separately on its two parameters (β and τ_β) at low frequencies (but only on the ratio β/τ_β at high frequencies), the β value obtained in this way converges well as data points are successively removed from the high-frequency end. In most cases, β did not change significantly if one more or one less data point was included in the fit.

High-frequency dispersion

The second free parameter in the constrained Lorentzian fit should be interpreted as $\alpha + \gamma\tau_\beta$, since it includes the low-frequency limit of the γ dispersion (cf. equation (3)). The three parameters in this combination clearly cannot be separated by the two or three additional high-frequency points. If a bi-Lorentzian fit is performed (including all data points) with β and τ_β fixed at their previously determined values, τ_γ will be rather well determined but α and γ couple strongly, and therefore cannot be individually determined. By making certain assumptions about α , however, we can obtain a useful estimate of γ . Since α is due to water molecules at the protein surface (Halle *et al.*, 1999), we require this parameter to have the same value for the apo and holo forms. Furthermore, we assume that the ratio $\alpha/R_{1,\text{bulk}}$ is the same for ^2H and ^{17}O , as it is for other proteins (Denisov & Halle, 1996). Finally, for batch II at 27 °C, we fix α to the value obtained by setting $N_\alpha = 460$ (see Results) and $\rho_\alpha = 4.5$, the mean value for seven other proteins at this temperature (Denisov & Halle, 1996). At 4 °C, $\alpha/R_{1,\text{bulk}}$ should be larger, since the activation enthalpy of rotation is higher for hydration water than

for bulk water (Denisov & Halle, 1998). We obtain α at 4 °C by requiring the mean value of γ to be the same at the two temperatures. We then fix α to its mean value for a given batch and redetermine γ and τ_γ from bi-Lorentzian fits with only two free parameters. The impurity in batch I will increase α due to direct hydration effects and, in the ^2H case, due to labile hydrogen atoms in the polybasic impurity. The labile hydrogen contribution will be largest at 27 °C, where hydrogen exchange is faster than at 4 °C. For batch I samples, the fixed α value was determined in a similar way by requiring the mean value of γ to be the same in the two batches at a given temperature.

The final two-parameter constrained bi-Lorentzian fits are virtually indistinguishable from five-parameter unconstrained bi-Lorentzian fits. The rather elaborate protocol of constrained fits described here, however, has two advantages. First, and most importantly, it uses independent information (about τ_R and its temperature dependence) and the frequency separation inherent in the dispersion profile to determine the crucial β parameter as accurately as possible. Second, by invoking independent information about α , it provides an estimate of γ . Since the assumptions about α are less secure, only semiquantitative significance should be attached to the derived γ values. The relative variation in γ on ligand binding, however, should be more reliable.

Acknowledgments

In Lund, we thank Vladimir Denisov, Haukur Jóhannesson, Kristofer Modig, and Eva Thulin for assistance with NMR spectrometers and protein purification. In Rochester, we thank Vladimir Likic, Nenad Juranic, and Slobodan Macura for making available their water-NOE results on ANS-IFABP, and Vladimir Likic for communicating his MD results. This work was supported by the Crafoord Foundation and the Swedish Natural Science Research Council (to B.H.) and by the National Institutes of Health, grant GM 34847 (to F.G.P.).

References

- Abraham, A. (1961). *The Principles of Nuclear Magnetism*, Clarendon Press, Oxford.
- Baker, E. N. (1995). Solvent interactions with proteins as revealed by X-ray crystallographic studies. In *Protein-Solvent Interactions* (Gregory, R. B., ed.), pp. 143-189, M. Dekker, New York.
- Banaszak, L., Winter, N., Xu, Z., Bernlohr, D. A., Cowan, S. & Jones, T. A. (1994). Lipid-binding proteins: a family of fatty acid and retinoid transport proteins. *Advan. Protein Chem.* **45**, 89-151.
- Cistola, D. P. & Hall, K. B. (1995). Probing internal water molecules in proteins using two-dimensional ^{19}F - ^1H NMR. *J. Biomol. NMR*, **5**, 415-419.
- Cistola, D. P., Kim, K., Rogl, H. & Frieden, C. (1996). Fatty acid interactions with a helix-less variant of intestinal fatty acid-binding protein. *Biochemistry*, **35**, 7559-7565.
- Denisov, V. P. & Halle, B. (1995a). Protein hydration dynamics in aqueous solution: a comparison of bovine pancreatic trypsin inhibitor and ubiquitin by oxygen-17 spin relaxation dispersion. *J. Mol. Biol.* **245**, 682-697.

- Denisov, V. P. & Halle, B. (1995b). Hydrogen exchange and protein hydration: the deuterium spin relaxation dispersions of bovine pancreatic trypsin inhibitor and ubiquitin. *J. Mol. Biol.* **245**, 698-709.
- Denisov, V. P. & Halle, B. (1996). Protein hydration dynamics in aqueous solution. *Faraday Discuss.* **103**, 227-244.
- Denisov, V. P. & Halle, B. (1998). Thermal denaturation of ribonuclease A characterized by water ^{17}O and ^2H magnetic relaxation dispersion. *Biochemistry*, **37**, 9595-9604.
- Denisov, V. P., Jonsson, B.-H. & Halle, B. (1999). Hydration of denatured and molten globule proteins. *Nature Struct. Biol.* In the press.
- Eads, J., Sacchettini, J. C., Kromminga, A. & Gordon, J. I. (1993). *Escherichia coli*-derived rat intestinal fatty acid binding protein with bound myristate at 1.5 Å resolution and I-FABP^{Arg106 → Gln} with bound oleate at 1.74 Å resolution. *J. Biol. Chem.* **268**, 26375-26385.
- Ernst, J. A., Clubb, R. T., Zhou, H. X., Gronenborn, A. M. & Clore, G. M. (1995). Demonstration of positionally disordered water within a protein hydrophobic cavity by NMR. *Science*, **267**, 1813-1817.
- Frolov, A. & Schroeder, F. (1997). Time-resolved fluorescence of intestinal and liver fatty acid binding proteins: role of fatty acyl CoA and fatty acid. *Biochemistry*, **36**, 505-517.
- Glatz, J. F. C. & van der Vusse, G. J. (1996). Cellular fatty acid-binding proteins: their function and physiological significance. *Prog. Lipid Res.* **35**, 243-282.
- Halle, B. & Wennerström, H. (1981). Nearly exponential quadrupolar relaxation. A perturbation treatment. *J. Magn. Reson.* **44**, 89-100.
- Halle, B., Denisov, V. P. & Venu, K. (1999). Multinuclear relaxation dispersion studies of protein hydration. In *Modern Techniques in Protein NMR* (Berliner, L. J. & Krishna, N. R., eds), vol. 17, Plenum, New York.
- Hodsdon, M. E. & Cistola, D. P. (1997a). Discrete backbone disorder in the nuclear magnetic resonance structure of apo intestinal fatty acid-binding protein: implications for the mechanism of ligand entry. *Biochemistry*, **36**, 1450-1460.
- Hodsdon, M. E. & Cistola, D. P. (1997b). Ligand binding alters the backbone mobility of intestinal fatty acid-binding protein as monitored by ^{15}N NMR relaxation and ^1H exchange. *Biochemistry*, **36**, 2278-2290.
- Hodsdon, M. E., Ponder, J. W. & Cistola, D. P. (1996). The NMR solution structure of intestinal fatty acid-binding protein complexed with palmitate: application of a novel distance geometry algorithm. *J. Mol. Biol.* **264**, 585-602.
- Hubbard, S. J. & Argos, P. (1995). Detection of internal cavities in globular proteins. *Protein Eng.* **8**, 1011-1015.
- Kirk, W. R., Kurian, E. & Prendergast, F. G. (1996). Characterization of the sources of protein-ligand affinity: 1-sulfonato-8-(1')anilinonaphthalene binding to intestinal fatty acid binding protein. *Biophys. J.* **70**, 69-83.
- Kurian, E. (1998). Solution structure of intestinal fatty acid binding protein complexed with 1-anilino-naphthalene-8-sulfonate: implications for ligand binding. *PhD thesis*, Mayo Foundation, Rochester, MN.
- Kurian, E., Kirk, W. R. & Prendergast, F. G. (1996). Affinity of fatty acid for rRat intestinal fatty acid binding protein: further examination. *Biochemistry*, **35**, 3865-3874.
- Lankhorst, D., Schriever, J. & Leyte, J. C. (1983). An NMR relaxation study of hydrogen exchange and its deuterium isotope effects in aqueous carboxylic acid solutions. *Chem. Phys.* **77**, 319-340.
- Liepinsh, E. & Otting, G. (1996). Proton exchange rates from amino acid side chains-Implications for image contrast. *Magn. Reson. Med.* **35**, 30-42.
- Mesgarzadeh, A., Pfeiffer, S., Engelke, J., Lassen, D. & Rüterjans, H. (1998). Bound water in apo and holo bovine heart fatty-acid-binding protein determined by heteronuclear NMR spectroscopy. *Eur. J. Biochem.* **251**, 781-786.
- Nicholls, A., Bharadwaj, R. & Honig, B. (1993). GRASP: graphical representation and analysis of surface properties. *Biophys. J.* **64**, 166-170.
- Otting, G. (1997). NMR studies of water bound to biological molecules. *Progr. NMR Spectrosc.* **31**, 259-285.
- Otting, G., Liepinsh, E., Halle, B. & Frey, U. (1997). NMR identification of hydrophobic cavities with low water occupancies in protein structures using small gas molecules. *Nature Struct. Biol.* **4**, 396-404.
- Press, W. H., Flannery, B. P., Teukolsky, S. A. & Vetterling, W. T. (1986). *Numerical Recipes. The Art of Scientific Computing*, Cambridge University Press, Cambridge.
- Rashin, A. A., Iofin, M. & Honig, B. (1986). Internal cavities and buried waters in globular proteins. *Biochemistry*, **25**, 3619-3625.
- Richieri, G. V., Ogata, R. T. & Kleinfeld, A. M. (1995). Thermodynamics of fatty acid binding to fatty acid-binding proteins and fatty acid partition between water and membranes measured using the fluorescent probe ADIFAB. *J. Biol. Chem.* **270**, 15076-15084.
- Richieri, G. V., Ogata, R. T. & Kleinfeld, A. M. (1996). Kinetics of fatty acid interactions with fatty acid-binding proteins from adipocyte, heart, and intestine. *J. Biol. Chem.* **271**, 11291-11300.
- Richieri, G. V., Low, P. J., Ogata, R. T. & Kleinfeld, A. M. (1997). Mutants of rat intestinal fatty acid-binding protein illustrate the critical role played by enthalpy-entropy compensation in ligand binding. *J. Biol. Chem.* **272**, 16737-16740.
- Richieri, G. V., Low, P. L., Ogata, R. T. & Kleinfeld, A. M. (1998). Thermodynamics of fatty acid binding to engineered mutants of the adipocyte and intestinal fatty acid-binding proteins. *J. Biol. Chem.* **273**, 7397-7405.
- Sacchettini, J. C. & Gordon, J. I. (1993). Rat intestinal fatty acid binding protein. *J. Biol. Chem.* **268**, 18399-18402.
- Sacchettini, J. C., Gordon, J. I. & Banaszak, L. J. (1989a). Crystal structure of rat intestinal fatty acid-binding protein. *J. Mol. Biol.* **208**, 327-339.
- Sacchettini, J. C., Gordon, J. I. & Banaszak, L. J. (1989b). Refined apoprotein structure of rat intestinal fatty acid binding protein produced in *Escherichia coli*. *Proc. Natl Acad. Sci. USA*, **86**, 7736-7740.
- Sacchettini, J. C., Scapin, G., Gopaul, D. & Gordon, J. I. (1992). Refinement of the structure of *Escherichia coli*-derived rat intestinal fatty acid binding protein with bound oleate to 1.75-Å resolution. Correlation with the structures of the apoprotein and the protein with bound palmitate. *J. Biol. Chem.* **267**, 23534-23545.
- Scapin, G., Gordon, J. I. & Sacchettini, J. C. (1992). Refinement of the structure of recombinant rat intestinal fatty acid-binding apoprotein at 1.2-Å resolution. *J. Biol. Chem.* **267**, 4253-4269.

- Sobol, A. G., Wider, G., Iwai, H. & Wüthrich, K. (1998). Solvent magnetization artifacts in high-field NMR studies of macromolecular hydration. *J. Magn. Reson.* **130**, 262-271.
- Williams, M. A., Goodfellow, J. M. & Thornton, J. M. (1994). Buried waters and internal cavities in monomeric proteins. *Protein Sci.* **3**, 1224-1235.
- Woolf, T. B. (1998). Simulations of fatty acid-binding proteins suggest sites important for function. I. Stearic acid. *Biophys. J.* **74**, 681-693.
- Woolf, T. B. & Tychko, M. (1998). Simulations of fatty acid-binding proteins II. Sites for discrimination of monounsaturated ligands. *Biophys. J.* **74**, 694-707.
- Young, A. C. M., Scapin, Q., Kromminga, A., Patel, S. B., Veerkamp, J. H. & Sacchettini, J. C. (1994). Structural studies on human muscle fatty acid binding protein at 1.4 Å resolution: binding interactions with three C18 fatty acids. *Structure*, **2**, 523-534.

Edited by P. E. Wright

(Received 28 August 1998; received in revised form 6 November 1998; accepted 10 December 1998)